Catalyzed Chemoselective Acrolein Hydrogenation. Density Functional Studies

Chun-Fang Huo,[†] Yong-Wang Li,[†] Matthias Beller,[‡] and Haijun Jiao*[,†,‡]

The State Key Laboratory of Coal Conversion, Institute of Coal Chemistry, Chinese Academy of Sciences, Taiyuan 030001, People's Republic of China, and Leibniz-Institut für Organische Katalyse an der Universität Rostock e.V., Buchbinderstrasse 5-6, 18055 Rostock, Germany

Received November 24, 2003

The catalytic chemoselective hydrogenation of C═O and C═C bonds of acrolein by $HCo(CO)_3$ has been investigated at the B3LYP density functional level of theory. For the C═O hydrogenation to allyl alcohol, it is found that the reaction path with the allyloxy intermediate is more favored than the alternative path with the hydroxyallyl intermediate both kinetically and thermodynamically. For the C═C hydrogenation to propanal, the reaction path of the hydride transfer to C_β is more favored than to C_α by the lower barrier of the Co−H insertion and the overall lower free energy barriers. The larger stability of the π complex $HCo(CO)_3$-(η^2-H_2C═CHCHO) determines the C═C chemoselectivity. Thus, propanal is the expected principal product, while the formation of allyl alcohol is almost suppressed, in line with the experimental finding.

Introduction

Hydrogenation of α,β-unsaturated aldehydes is not only of great importance in industry[1−3] but also of specific scientific interest.[4] α,β-Unsaturated aldehydes can be transformed selectively to unsaturated alcohols or saturated aldehydes. In general, C═C bonds are more reactive than C═O bonds in hydrogenation both thermodynamically and kinetically,[5] and the former can be readily achieved under mild conditions with high selectivity for saturated aldehydes.[6] Since unsaturated alcohols are valuable intermediates or products such as flavors and perfumes in fine chemicals and pharmacy,[1,5] the development of reliable hydrogenation catalysts with excellent carbonyl selectivity has become one of the most challenging projects.

Despite some homogeneous[7−11] and heterogeneous[5,12−15] catalysts reported to affect C═O bonds selectivity, most of them have the limitation of reaction substrates and reducing agents. Grosselin et al.[7] found that the selectivity depends highly on the nature of catalysts. For example, α,β-unsaturated aldehydes could be reduced either into allylic alcohols with the Ru/TPPTS system or into saturated aldehydes with Rh/TPPTS. Ohkuma et al.[8] reported a combined catalyst system $RuCl_2(P(C_6H_5)_3)_3$ and $NH_2(CH_2)_2NH_2$/KOH with excellent capability of selective carbonyl hydrogenation for a wide range of carbonyl compounds possessing an olefinic or acetylenic bond. It is found that $RuCl_2$-$(P(C_6H_5)_3)_3$ is effective for olefin hydrogenation, but is very poor for carbonyl hydrogenation. The combined effects of $NH_2(CH_2)_2NH_2$ and KOH decelerate the catalyzed olefin hydrogenation by $RuCl_2(P(C_6H_5)_3)_3$ and, in turn, accelerate carbonyl hydrogenation. For the supported metal catalysts, e.g., Pt, Co, Rh, or Au, the selection of promoters, supports, and reduction conditions is important for the selective formation of unsaturated alcohol.[12] Using infrared spectra, Bailie et al.[13] characterized the active sites and poisoning of cobalt surface sites in Co/SiO_2 catalyst and showed that low-coordination edge or step sites in high-index planes containing Co^{n+} and Co^0 are active for C═O hydrogenation, but completely poisoned by SO_2. Marinelli et al.[14] and Ando et al.[15] discussed the influence of substituents at the α- and/or β-position of acrolein for the selectivity to unsaturated alcohol. They found that the selectivity depends strongly on the steric hindrance around the C═C bonds, and substituents at the β-position prevent the hydrogenation more effectively. They also attributed the high selectivity to the dominant adsorption of the C═O bond on the active center of the catalysts. In the

* Corresponding author. E-mail: hjiao@ifok.uni-rostock.de.
[†] The State Key Laboratory of Coal Conversion.
[‡] Leibniz-Institut für Organische Katalyse an der Universität Rostock e.V.

(1) (a) Gallezot, P.; Giroir-Fendler, A.; Richard, D. *Catalysis of Organic Reactions*; Marcel Dekker: New York, 1991. (b) Augustine, R. L. *Heterogeneous Catalysts in Organic Synthesis*; Dekker: New York, 1995.
(2) Coq, B.; Figueras, F. *Coord. Chem. Rev.* **1998**, *178−180*, 1753.
(3) Gallezot, P.; Richard, D. *Catal. Rev. Sci. Eng.* **1998**, *40*, 81.
(4) Claus, P. *Topics in Catalysis*; Special Issue *Fine Chemicals Catalysis, Part II*; Somorjai, G. A., Thomas, J. M., Blackmond, D., Leitner, W., Eds.; Baltzer Science Publishers: Bussum, The Netherlands, 1998; Vol. 5.
(5) Mohr, C.; Hofmeister, H.; Radnik, J.; Claus, P. *J. Am. Chem. Soc.* **2003**, *125*, 1905.
(6) Rylander, P. N. *Catalytic Hydrogenation in Organic Synthesis*; Academic Press: New York, 1979.
(7) Grosselin, J. M.; Mercier, C.; Allmang, G.; Grass, F. *Organometallics* **1991**, *10*, 2126.
(8) Ohkuma, T.; Ooka, H.; Ikariya, T.; Noyori, R. *J. Am. Chem. Soc.* **1995**, *117*, 10417.
(9) Kaneda, K.; Mizugaki, T. *Organometallics* **1996**, *15*, 3247.
(10) Mizugaki, T.; Kanayama, Y.; Ebitani, K.; Kaneda, K. *J. Org. Chem.* **1998**, *63*, 2378.
(11) Chen, J.-X.; Daeuble, J. F.; Brestensky, D. M.; Stryker, J. M. *Tetrahedron* **2000**, *56*, 2153.
(12) Shirai, M.; Tanaka, T.; Arai, M. *J. Mol. Catal. A* **2001**, *168*, 99.
(13) Bailie, J. E.; Rochester, C. H.; Hutchings, G. J. *J. Mol. Catal. A* **1998**, *136*, 35.
(14) Marinelli, T. B. L. W.; Naarburs, S.; Ponec, V. *J. Catal.* **1995**, *151*, 431.
(15) Ando, C.; Kurokawa, H.; Miura, H. *Appl. Catal. A* **1999**, *185*, L181.

10.1021/om034317u CCC: $27.50
Publication on Web 03/31/2004

latest work, acrolein hydrogenation to allyl alcohol, which is considered the most difficult to be realized due to lack of space-filling substituents at the C═C group, was investigated on Au/ZnO catalyst by Mohr et al.,[5] and the correlation between surface structure and catalytic behavior reveals the edges of single crystalline gold particles to be the active sites for the preferred C═O hydrogenation.

Transition metal hydrides are known to be active catalysts widely used in organic synthesis and industry, of which hydroformylation is one of the most representative examples. Since its discovery by Roelen in 1938, hydroformylation has developed into an important industrial process to convert olefins and synthesis gas into aldehydes.[16−22] However, taking alkynes as feedstocks, the products of hydroformylation are complicated. Accompanied with the variation of catalysts, reactants, and reaction conditions, the main products may be unsaturated aldehydes,[23−25] saturated aldehydes, unsaturated alcohols, saturated alcohols, or their mixtures.[26−33] This can be attributed to two potential reasons: (a) alkyne hydrogenation prior to hydroformylation and (b) the hydrogenation of the initially formed unsaturated aldehydes, as shown in reaction eqs 1−5.

$$RC{\equiv}CR' + CO + H_2 \rightarrow RHC{=}CR'CHO \quad (1)$$

$$RC{\equiv}CR' + H_2 \rightarrow RHC{=}CHR' \quad (2)$$

$$RHC{=}CHR' + CO + H_2 \rightarrow RH_2CCHR'CHO \quad (3)$$

$$RHC{=}CR'CHO + H_2 \rightarrow RHC{=}CR'CH_2OH \quad (4)$$

$$RHC{=}CR'CHO + H_2 \rightarrow RH_2CCHR'CHO \quad (5)$$

In our previous work, the mechanism of the $HCo(CO)_3$-catalyzed acetylene hydroformylation to acrolein has been investigated with the B3LYP density functional method.[34] It was verified that acetylene hydrogenation (2) is not competitive to hydroformylation (1) under stoichometric conditions, and therefore the subsequent reaction 3 is unlikely. In addition, it was pointed out that acrolein can be further hydrogenated to saturated aldehyde or alcohol. The goal of our present work is the exploring of the detailed reaction pathways of acrolein hydrogenation under $HCo(CO)_3$-catalyzed hydroformylation conditions (reactions 4 and 5). The origin of the chemoselectivity has been discussed for the design of highly selective catalysts.

Computational Details

All calculations were performed at the B3LYP/6-311+G(d)[35] density functional level of theory with the Gaussian 98 program.[36] The structures of intermediates and transition states were fully optimized, without any symmetry constraints. The frequency analyses were carried out at the same level to confirm that the optimized structures were ground states without imaginary frequency (NImag = 0) or transition states (TS) with one imaginary frequency (NImag = 1) on the potential energy surface (PES). Especially, the lone imaginary frequency of each transition state displayed the desired displacement orientation, and the validity of each reaction path was further examined by the intrinsic reaction coordinate calculations. The enthalpies and the Gibbs free energies[37] were calculated at the actual reaction conditions of 403.15 K and 200 atm. Considering the entropies, our discussions are based on the free energies (ΔG) of activation and reaction, and the corresponding enthalpies (ΔH) are provided in square brackets in the energy profiles for comparison. The calculated total electronic energies, ZPEs, and thermal corrections to enthalpies and Gibbs free energies are provided in the Supporting Information.

Results and Discussion

Acrolein is a difunctional compound. Either C═O or C═C bonds can be activated via coordination to the catalyst $HCo(CO)_3$. As depicted in Scheme 1, four reaction pathways are possible. Along paths A and B, allyl alcohol ($H_2C{=}CH{-}CH_2OH$) is formed by selective hydrogenation of the C═O bond. As an alternative case, the selective hydrogenation of the C═C group goes through paths C and D, leading to propanal (CH_3CH_2CHO). It is clearly shown that each reaction path involves four elementary steps, (i) acrolein coordination, (ii) hydride transfer to acrolein, (iii) H_2 oxidative addition, and (iv) reductive elimination of allyl alcohol or propanal with catalyst regeneration. In the following

(16) (a) van Leeuwen, P. W. N. M.; Claver, C. *Rhodium Catalyzed Hydroformylation*; Kluwer Academic Publishers: Dordrecht, The Netherlands, 2000. (b) Falbe, J. *New Sytheses with Carbon Monoxide*; Springer-Verlag: Berlin, 1980. (c) Torrent, M.; Solà, M.; Frenking, G. *Chem. Rev.* **2000**, *100*, 439.
(17) Beller, M.; Cornils, B.; Frohning, C. D.; Kohlpaintner, C. W. *J. Mol. Catal. A* **1995**, *104*, 17.
(18) Parshall, G. W.; Ittel, S. D. *Homogeneous Catalysis*; Wiley-Interscience: New York, 1992.
(19) Cornils, B.; Herrmann, W. A. *Applied Homogeneous Catalysis with Organometallic Compounds*; Wiley-VCH: Weinheim, 2002; Vol. 1.
(20) Orchin, M.; Rupilius, W. *Catal. Rev.* **1972**, *6*, 85.
(21) Süss-Fink, G.; Meister, G. *Adv. Organomet. Chem.* **1993**, *35*, 41.
(22) Papadogianakis, G.; Sheldon, R. A. *New J. Chem.* **1996**, *20*, 175.
(23) Johnson, J. R.; Cuny, G. D.; Buchwald, S. L. *Angew. Chem., Int. Ed. Engl.* **1995**, *34*, 1760.
(24) Ishii, Y.; Miyashita, K.; Kamita, K.; Hidai, M. *J. Am. Chem. Soc.* **1997**, *119*, 6448.
(25) Van den Hoven, B. G.; Alper, H. *J. Org. Chem.* **1999**, *64*, 9640.
(26) Natta, G.; Pino, P. *The 12th International Congress of Pure and Applied Chemistry*; New York, September 1951.
(27) Greenfield, H.; Wotiz, J. H.; Wender, I. *J. Org. Chem.* **1957**, *22*, 542.
(28) Fell, B.; Beutler, M. *Tetrahedron Lett.* **1972**, *13*, 3455.
(29) Botteghi, C.; Salomon, Ch. *Tetrahedron Lett.* **1974**, *15*, 4285.
(30) Doyama, K.; Joh, T.; Shiohara, T.; Takahashi, S. *Bull. Chem. Soc. Jpn.* **1988**, *61*, 4353.
(31) Wuts, P. G. M.; Ritter, A. R. *J. Org. Chem.* **1989**, *54*, 5180.
(32) Campi, E. M.; Jackson, W. R.; Nilsson, Y. *Tetrahedron Lett.* **1991**, *32*, 1093.
(33) Nombel, P.; Lugan, N.; Mulla, F.; Lavigne, G. *Organometallics* **1994**, *13*, 4673.
(34) Huo, C.-F.; Li, Y.-W.; Beller, M.; Jiao, H. *Organometallics* **2004**, *23*, 765.
(35) (a) Becke, A. D. *J. Chem. Phys.* **1993**, *98*, 5648. (b) Stevens, P. J.; Devlin, F. J.; Chablowski, C. F.; Frisch, M. J. *J. Phys. Chem.* **1994**, *98*, 11623.
(36) Frisch, M. J.; Trucks, G. W.; Schlegel, H. B.; Scuseria, G. E.; Robb, M. A.; Cheeseman, J. R.; Zakrzewski, V. G.; Montgomery, J. A.; Stratmann, R. E.; Burant, J. C.; Dapprich, S.; Millam, J. M.; Daniels, A. D.; Kudin, K. N.; Strain, M. C.; Farkas, O.; Tomasi, J.; Barone, V.; Cossi, M.; Cammi, R.; Mennucci, B.; Pomelli, C.; Adamo, C.; Clifford, S.; Ochterski, J.; Petersson, G. A.; Ayala, P. Y.; Cui, Q.; Morokuma, K.; Malick, D. K.; Rabuck, A. D.; Raghavachari, K.; Foresman, J. B.; Cioslowski, J.; Ortiz, J. V.; Stefanov, B. B.; Liu, G.; Liashenko, A.; Piskorz, P.; Komaromi, I.; Gomperts, R.; Martin, R. L.; Fox, D. J.; Keith, T.; Al-Laham, M. A.; Peng, C. Y.; Nanayakkara, A.; Gonzalez, C.; Challacombe, M.; Gill, P. M. W.; Johnson, B. G.; Chen, W.; Wong, M. W.; Andres, J. L.; Head-Gordon, M.; Replogle, E. S.; Pople, J. A. *Gaussian 98*; Gaussian, Inc.: Pittsburgh, PA, 1998.
(37) Ochterski, J. W. *Thermochemistry in Guassian* (see: help@Gaussian.com).

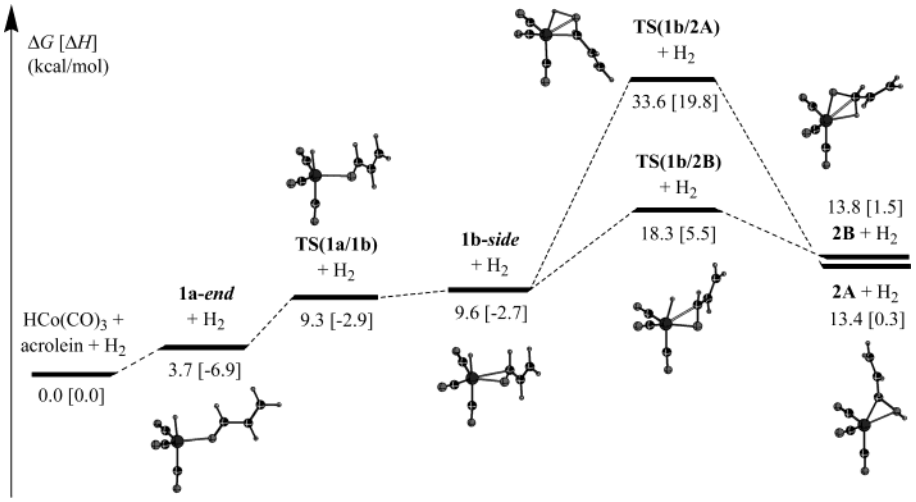

Figure 1. Free energy profiles (kcal/mol, enthalpies in square brackets) for acrolein coordination via the C═O bond and C═O insertion into the Co−H bond (relative to $HCo(CO)_3$ + acrolein + H_2).

Scheme 1. Proposed Reaction Pathways for the Selective Hydrogenation of Acrolein

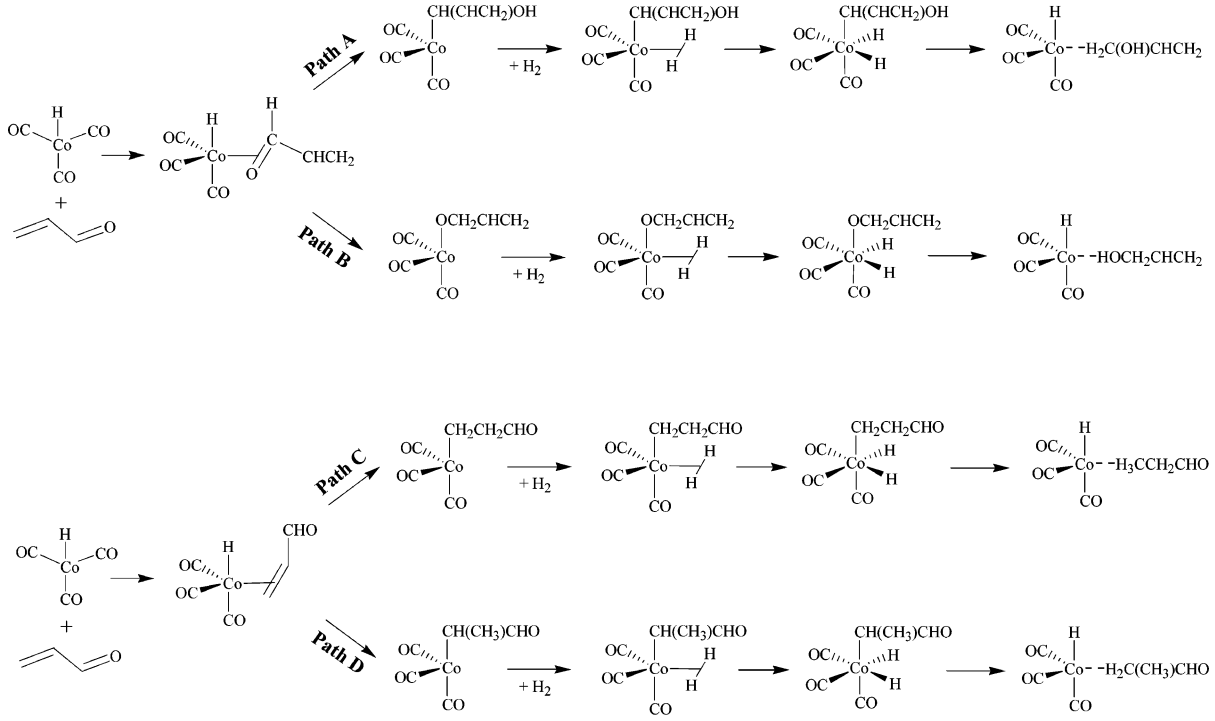

section, the structures and energies of the intermediates and transition states involved in the postulated steps are discussed first, and then the free energy surface is constructed for each reaction path. In light of these results, the chemoselectivity is addressed.

(1) Selective Hydrogenation of the C═O Bond. (a) Acrolein Coordination. Acrolein coordination to $HCo(CO)_3$ via a formyl group can adopt two key modes, i.e., (i) *end-on* coordination by a lone pair of the oxygen atom and (ii) *side-on* coordination through the C═O π orbital. The free energy profile for this process is reported on the left side of Figure 1, and the optimized structures are illustrated in Figure 2.

Due to the planar C_{2v} $HCo(CO)_3$ form,[38] the incoming acrolein attacks the equatorial site, forming the trigonal bipyramid complexes. As shown in Figure 1, complex **1a-*end*** is more stable than **1b-*side*** by 5.9 kcal/mol, and the former is obviously the favored coordinating mode. However, in **1b-*side***, the C═O bond is more activated than that in **1a-*end***, indicated by the longer C═O bond length (1.254 vs 1.224 Å) with respect to that of 1.211 Å in free acrolein. This suggests that **1b-*side*** facilitates the subsequent reaction of acrolein insertion into the Co−H bond. Furthermore, an interesting character of the π complex **1b-*side*** is that the oxygen atom of the formyl group is much closer to the cobalt center than the carbon atom by 0.208 Å. This behavior was observed in the few formaldehyde complexes for which structures have been determined experimentally.[39−41] For getting

(38) Huo, C.-F.; Li, Y.-W.; Wu, G.-S.; Beller, M.; Jiao, H. *J. Phys. Chem. A* **2002**, *106*, 12161.

(39) Gambarotta, S.; Floriani, C.; Chiesi-Villa, A.; Guastini, C. *J. Am. Chem. Soc.* **1985**, *107*, 2985.

(40) Gambarotta, S.; Floriani, C.; Chiesi-Villa, A.; Guastini, C. *J. Am. Chem. Soc.* **1982**, *104*, 2019.

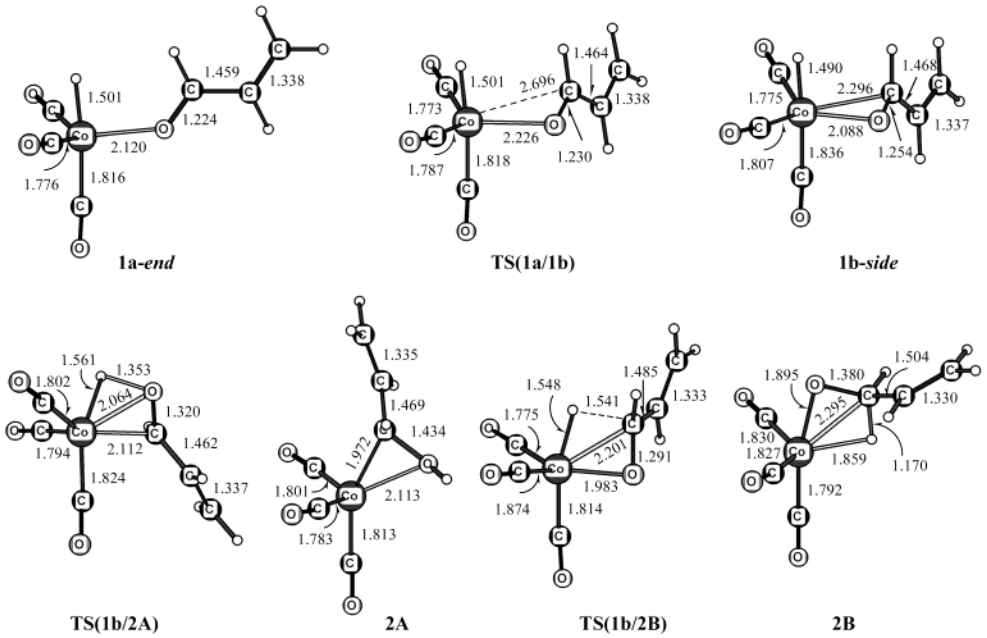

Figure 2. Bond parameters (in Å) of the critical points for acrolein coordination via the C═O bond and C═O insertion into the Co−H bond.

further insight into the PES, the corresponding transition state **TS(1a/1b)** was located. As depicted in Figure 2, accompanied with the transformation from *end-on* to *side-on* mode, the Co−O bond is stretched. Compared with the corresponding stable intermediates, **TS(1a/1b)** has the longest Co−O distance. The free energy profile in Figure 1 clearly shows that acrolein coordination to $HCo(CO)_3$ forming the most stable complex **1a-*end*** is endergonic by 3.7 kcal/mol, but exothermic by 6.9 kcal/mol. Furthermore, the transformation process requires the overcoming of a free energy barrier of 5.6 kcal/mol.

(b) C═O Insertion into the Co−H Bond. As described in Scheme 1, the insertion of the formyl group into the Co−H bond may occur via two channels, i.e., path A and path B. The hydride ligand shifts to the oxygen atom, resulting in the hydroxyallyl intermediate (**2A**), whereas the hydride transfers to the carbon atom, leading to the allyloxy intermediate (**2B**). The related free energy profiles are depicted on the right side of Figure 1, and the structures of the critical points are illustrated in Figure 2. Both **2A** and **2B** adopt the geometry derived from a trigonal bipyramid. In **2A**, the hydroxyallyl group is at the axial site with the oxygen atom of the hydroxyl group facing the free equatorial site and reacting with the cobalt center by the η^2-O−C interaction. In **2B**, the allyloxy group is at the axial site and stabilized by the Co···H−C agostic interaction in the vacant equatorial site. From the energy profiles in Figure 1, we can see that **2A** and **2B** are almost equal in free energy.

Taking the π complex **1b-*side*** as the starting point, the formation of **2A** and **2B** by the C═O insertion into the Co−H bond is investigated. We located two transition states, **TS(1b/2A)** and **TS(1b/2B)**, for these two channels, respectively. As illustrated in Figure 2, **TS(1b/2A)** and **TS(1b/2B)** have distorted square pyramidal geometries. An interesting feature of this reaction is the hydride migration coupled with the skeletal Berry pseudorotation. Therefore, the C═O insertion into the Co−H bond does not occur via a direct way. From the energy profiles in Figure 1, it is evident that the formation of both **2A** and **2B** is accessible thermodynamically. The former is endergonic by 3.8 kcal/mol, and the latter is endergonic by 4.2 kcal/mol. However, the formation of **2A** has a high free energy barrier of 24.0 kcal/mol, while a rather lower barrier of 8.7 kcal/mol is found for the formation of **2B**. From the kinetic point of view, the hydride transfer to carbon forming the allyloxy intermediate **2B** is more favored.

(c) H_2 Coordination and Oxidative Addition. The free energy profiles associated with this process are represented in Figure 3, whereas the detailed structures of the critical points are displayed in Figure 4. Since the formation of **2B** is more favored kinetically, the related process of **2B** is discussed first. Coordination of H_2 to **2B** leads to the dihydrogen complex **3Ba**, in which H_2 is in the equatorial plane in η^2 coordination. We have found that formation of **3Ba** favors the attachment of H_2 from the backside of the agostic bond in **2B** via the corresponding transition state **TS(2B/3Ba)**. From the free energy profile in Figure 3, one can see that H_2 coordination to **2B** is slightly endergonic by 5.0 kcal/mol. It is interesting to point out that **3Ba** is higher in energy than the corresponding transition state, and this indicates that this coordination is an endergonic process without additional barrier.

The following step is the H_2 oxidative addition of **3Ba** to the dihydride complex **3Bb**. As depicted in Figure 4, **3Bb** has a slightly distorted octahedral geometry, in which the axial group is bent toward the sterically less demanding hydride ligands. During the course of **3Ba** to **3Bb**, the H_2 oxidative addition couples with the allyloxy group rotation. Along the cleavage of H_2, the allyloxy group rotates about 37° in the corresponding transition state **TS(3Ba/3Bb)** and 180° in **3Bb**.

(41) Brown, K. L.; Clark, G. R.; Headford, C. E. L.; Marsden, K.; Roper, W. R. *J. Am. Chem. Soc.* **1979**, *101*, 503.

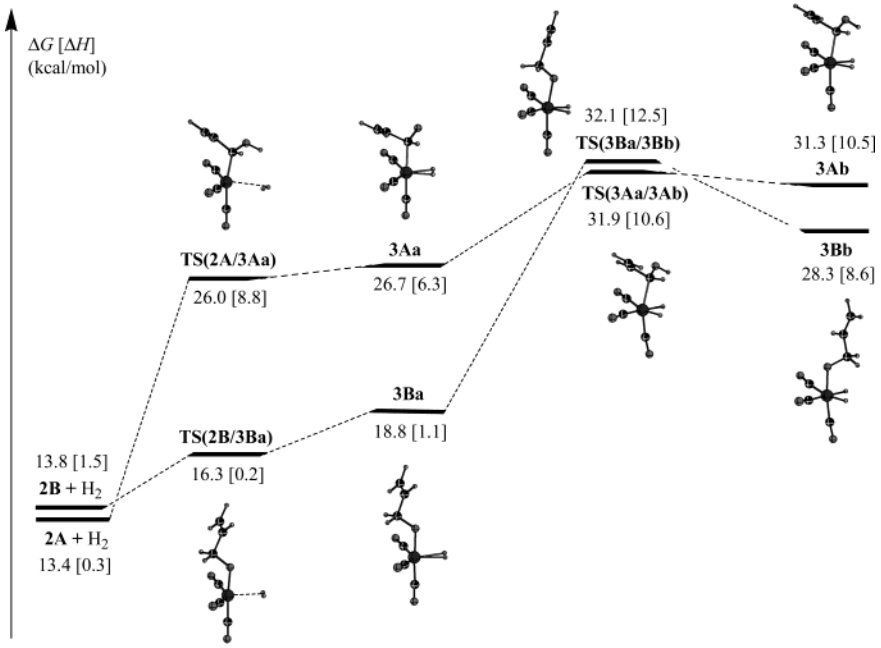

Figure 3. Free energy profiles (kcal/mol, enthalpies in square brackets) for H_2 coordination and the oxidative addition of C═O hydrogenation (relative to $HCo(CO)_3$ + acrolein + H_2).

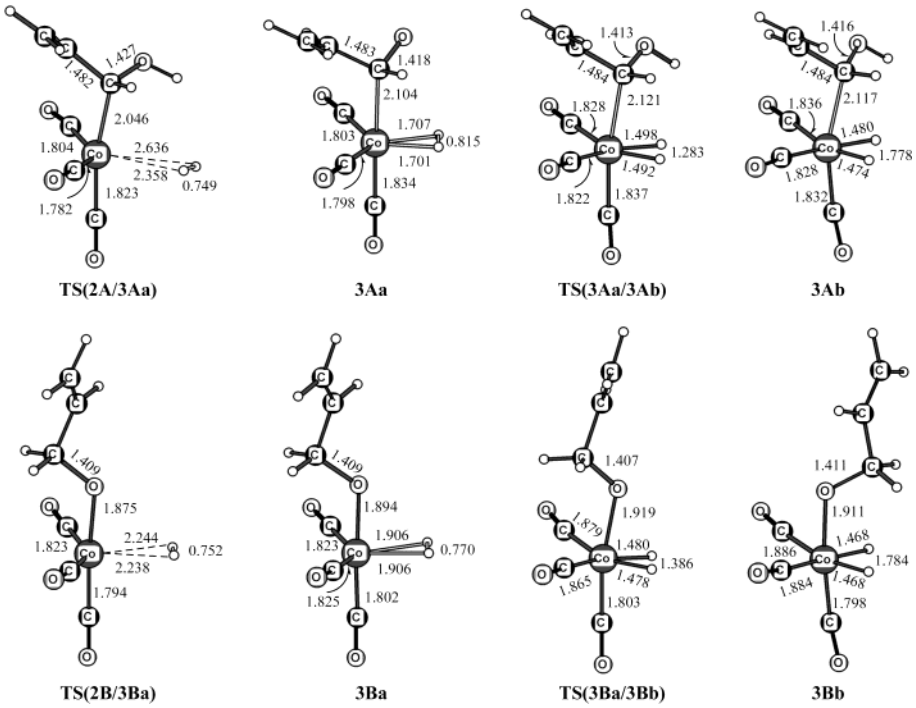

Figure 4. Bond parameters (in Å) of the critical points involved in H_2 coordination and the oxidative addition of C═O hydrogenation.

A similar process is found for the H_2 coordination to **2A**, but the formation of **3Aa** favors the attachment of H_2 from the front side of the O−C stabilized Co center via the related transition state **TS(2A/3Aa)**. In addition, **3Ba** is more stable than **3Aa** by 7.9 kcal/mol, indicating that the formation of **3Ba** is more favored thermodynamically. Furthermore, **3Bb** is also more stable than **3Ab** by 3.0 kcal/mol, but the formation of the former has a larger free energy barrier than the latter (13.3 vs 5.2 kcal/mol).

(d) Allyl Alcohol Elimination. The elimination of allyl alcohol from **3Ab** or **3Bb** proceeds by one of the hydride ligands migrating and attacking the corresponding carbon or oxygen atom. The free energy profiles for this step are given in Figure 5, while the related structures are illustrated in Figure 6. It is shown that this process proceeds via the three-center transition state, **TS(3Ab/4A)** or **TS(3Bb/4B)**, to the allyl alcohol adduct **4A** or **4B** (Figure 6). The allyl alcohol is attached to $HCo(CO)_3$ through the α hydrogen atom in an agostic interaction in **4A**, while via the hydrogen atom of hydroxyl group in **4B**. As depicted in Figure 5, the allyl alcohol elimination from **3Ab** or **3Bb** is highly exergonic by 25.1 or 24.1 kcal/mol, and the corresponding free energy barriers are 7.1 and 11.8 kcal/mol, respectively.

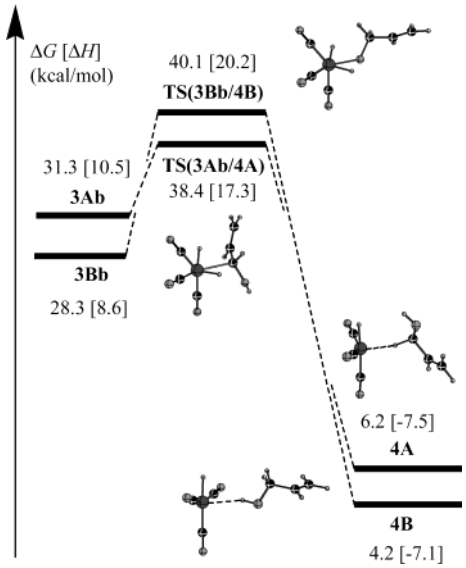

Figure 5. Free energy profiles (kcal/mol, enthalpies in square brackets) for allyl alcohol elimination (relative to $HCo(CO)_3$ + acrolein + H_2).

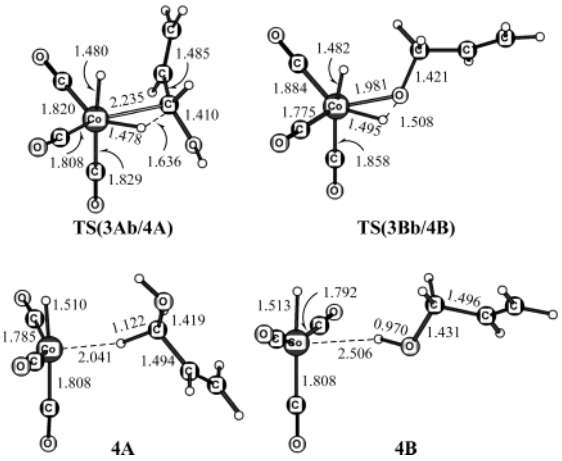

Figure 6. Bond parameters (in Å) of the critical points involved in allyl alcohol elimination.

(e) Reaction Pathways for Allyl Alcohol Formation. As mentioned above, hydrogenation of aldehyde to alcohol may proceed via the hydroxyalkyl or an alkoxy intermediate. Experimentally, different views are coexistent. Fahey[42] argued that the polarity of the Co−H bond might favor the formation of a hydroxyalkyl intermediate (like **2A**). However, Dombek[43] pointed out that in the cobalt-based catalytic hydroformylation of olefins the observed product distribution is consistent with a mechanism where most of the alcohol is produced via the alkoxy intermediate (like **2B**). In a pioneering theoretical study by Versluis and Ziegler,[44] the reaction profiles for formaldehyde insertion into the Co−H bond were modeled by a linear transit procedure and under C_s symmetry constraint. Despite the methodological limitations, they predicted a similar preference for forming methoxy and thus deduced that the catalytic conversion of aldehyde to alcohol most likely proceeds via an alkoxy intermediate. Nevertheless, in a subsequent study on the ethanol elimination from the hydrogenation of $CH_3(O)CCo(CO)_3$,[45] Solà and Ziegler did not take the alkoxy path into account.

Summarizing the results of each individual step discussed above, the most significant difference between these two pathways is the higher activation barrier during the Co−H insertion step for A than for B (24.0 vs 8.7 kcal/mol, Figure 1) and the overall more favored thermodynamic stability of the intermediates along B than along A (Figures 1, 3, and 5). Therefore, path B is a both kinetically and thermodynamically more favored C═O hydrogenation process via allyloxy intermediate, and path A is not competitive. For path B, the higher free energy barriers are related to the H_2 oxidative addition (**3Ba** → **3Bb**, 13.3 kcal/mol) and the allyl alcohol elimination (**3Bb** → **4B**, 11.8 kcal/mol). Therefore, both the H_2 oxidative addition and the allyl alcohol elimination are the rate-determining steps.

(2) Selective Hydrogenation of the C═C Bond. As the key step in hydroformylation, C═C bond coordination to $HCo(CO)_3$ and the subsequent Co−H insertion have been investigated at various levels of theory. The latest study focused on the regioselectivity of hydroformylation of propene.[46] Since both acrolein and propene can be considered as substituted olefins, the first two steps of the catalytic cycle are similar. The related results are discussed only briefly, and the differences are emphasized.

(a) Acrolein Coordination. Like propene, acrolein coordination to $HCo(CO)_3$ via the C═C bond forms the most stable π complexes $HCo(CO)_3(\eta^2$-$H_2C{=}CHCHO)$ (**1c-*syn*** and **1d-*anti***) with the C═C bond in the equatorial plane, and this process is slightly endergonic by 0.2 and 0.6 kcal/mol, while exothermic by 13.8 and 13.5 kcal/mol, respectively. The related structures involved in this process are shown in Figure 7. The free energy profile with the Newman projection in Figure 8 shows that the rotation barrier of acrolein is rather small, the same as propene.[46]

(b) C═C Insertion into the Co−H Bond. The insertion of acrolein (C═C) into the Co−H bond leading to formylalkyl complexes can take place in two ways (Scheme 1), i.e., the hydride transfer to HC═ (C_α, path C) and $H_2C{=}$ (C_β, path D). The free energy profiles for this process are reported in Figure 9, while the structures of the critical points are depicted in Figure 10. From the most stable complex **1d-*anti***, the Co−H insertion into C_α proceeds via a square pyramidal transition state, **TS(1d/2Ca)**, forming the Co···H−C_α agostic stabilized intermediate **2Ca**. During this pathway, the hydride transfer couples with a Berry pseudorotation of the skeleton. However, the hydride transfer to C_β is a stepwise process. First, **1d-*anti*** or **1c-*syn*** has to transform to **1f-*anti*** in order to bring the β-carbon into a position close to the hydride. Second, the insertion reaction occurs through a trigonal bipyramidal transition state, **TS(1f/2Da)**, leading to the Co···H−C_β agostic stabilized intermediate **2Da**. From the energy profiles in Figures 8 and 9, we can find that the formation of **2Ca** from **1d-*anti*** is slightly endergonic by 1.8 kcal/mol, while the formation of **2Da** from **1d-*anti*** or **1c-*syn*** is exergonic by 2.7 or 2.3 kcal/mol.

(42) Fahey, D. R. *J. Am. Chem. Soc.* **1981**, *103*, 136.
(43) Dombek, B. D. *Adv. Catal.* **1983**, *32*, 325.
(44) Versluis, L.; Ziegler, T. *J. Am. Chem. Soc.* **1990**, *112*, 6763.
(45) Solà M.; Ziegler, T. *Organometallics* **1996**, *15*, 2611.
(46) Huo, C.-F.; Li, Y.-W.; Beller, M.; Jiao, H. *Organometallics* **2003**, *22*, 4665.

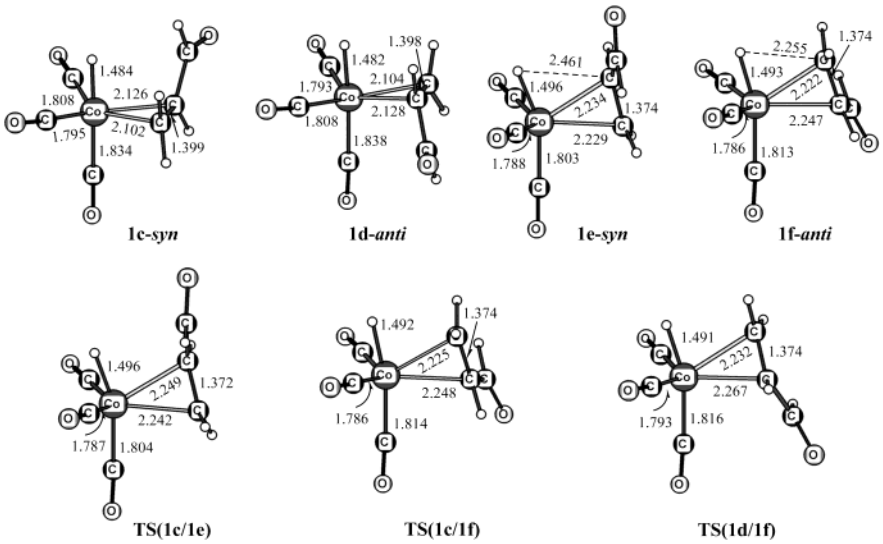

Figure 7. Bond parameters (in Å) of the critical points for acrolein coordination via the C═C bond.

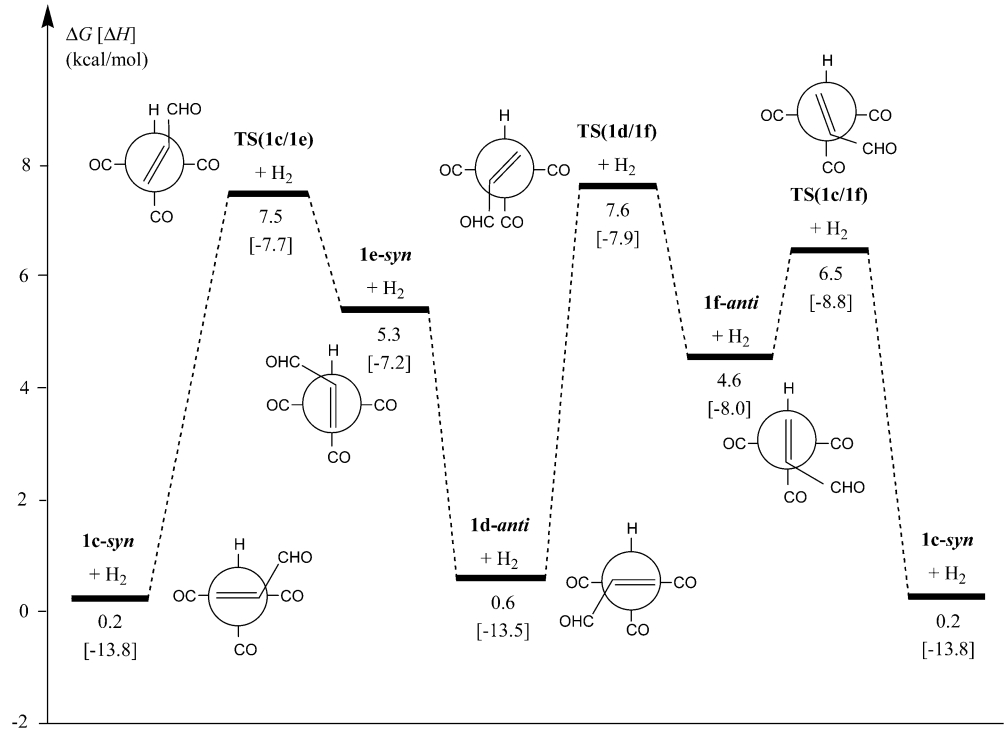

Figure 8. Free energy profile (kcal/mol, enthalpies in square brackets) with the Newman projection for acrolein coordination via the C═C bond (relative to $HCo(CO)_3$ + acrolein + H_2).

The following step is the further isomerization of **2Ca** or **2Da** to form the more stable conformation (**2Cb** or **2Db**), in which the oxygen atom of the formyl group participates in the coordination to $Co(CO)_3$. As illustrated in Figure 10, **2Cb** has a trigonal bipyramidal geometry with a η^2-coordination between $Co(CO)_3$ and the CH_2CH_2CHO group, while **2Db** has a square pyramidal geometry with a η^3-coordination between $Co(CO)_3$ and the CH_3CHCHO group. Furthermore, two related transition states for the rotation of the formylalkyl group, **TS(2Ca/2Cb)** and **TS(2Da/2Db)**, were located, which have butterfly geometries with an η^1-formylalkyl group at the axial site. As shown in Figure 9, η^2-complex **2Cb** and η^3-complex **2Db** are more stable than the corresponding agostic species **2Ca** and **2Da** by 4.0 and 5.9 kcal/mol, and the related conversion can be accomplished by overcoming a free energy barrier of 2.8 and 7.2 kcal/mol, respectively.

Interestingly, a comparison of the relative free energies of the corresponding isomers (**2Ca**/**2Da** and **2Cb**/**2Db**) presents a distinctly thermodynamic preference for **2Da** and **2Db** by 4.5 and 6.4 kcal/mol, which is in contrast to the related metal-propyl complex. For example, Decker and Cundari[47] studied propene insertion into the Rh−H bond of $HRh(PPh_3)_2(CO)(\eta^2\text{-}H_2C{=}CHCH_3)$ and found that the linear propyl conformers are 3−5 kcal/mol or 6−7 kcal/mol lower in energy than the corresponding branched conformers for the *cis* Rh-propyl or *trans* Rh-propyl species. On $HCo(CO)_3$-catalyzed propene hydroformylation, both propyl and

(47) Decker, S. A.; Cundari, T. R. *J. Organomet. Chem.* **2001**, *635*, 132.

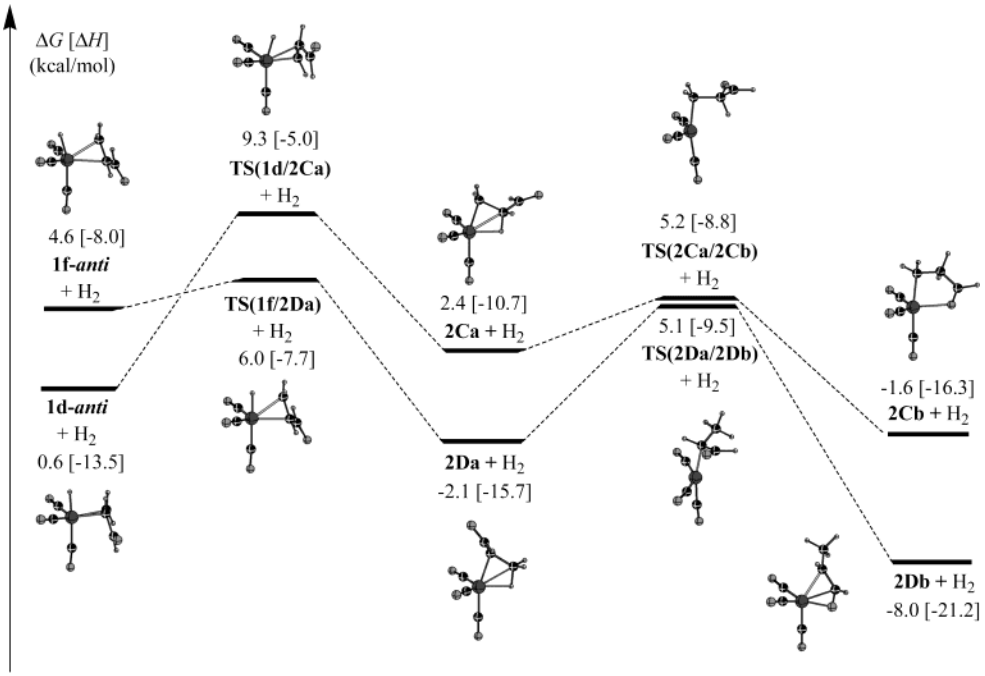

Figure 9. Free energy profiles (kcal/mol, enthalpies in square brackets) for C═C insertion into the Co−H bond (relative to $HCo(CO)_3$ + acrolein + H_2).

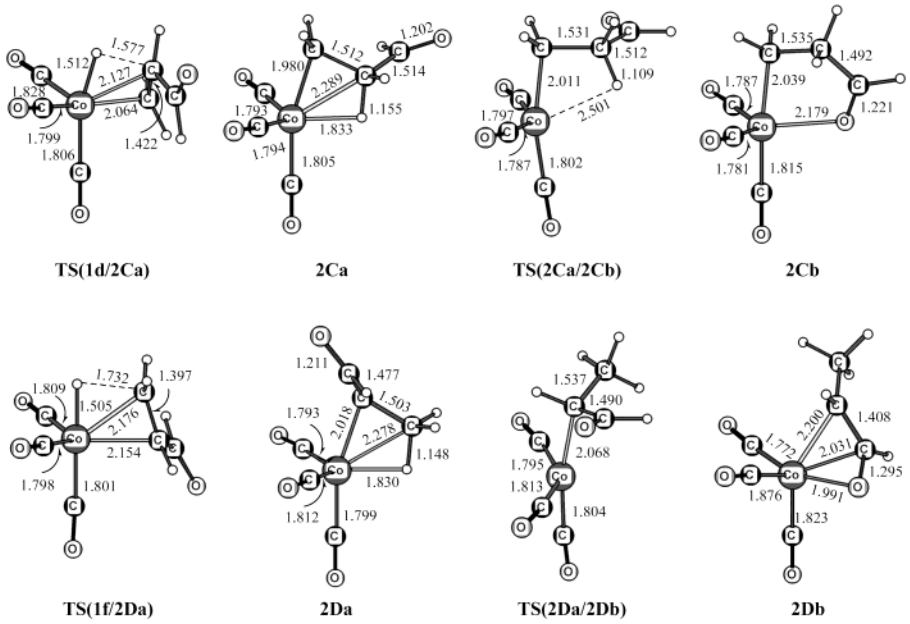

Figure 10. Bond parameters (in Å) of the critical points involved in C═C insertion into the Co−H bond.

isopropyl complexes ($RCo(CO)_3$) are very close in energy.[46] These results indicate that the substrate electronic structure imposes a strong influence on the migratory insertion direction. For acrolein insertion into the Co−H bond, the hydride transfer to the β-carbon is more favorable.

(c) H_2 Coordination and Oxidative Addition. The free energy profiles for this process are represented in Figure 11, whereas the detailed structures of the critical points are depicted in Figure 12. H_2 coordination to **2Cb** and **2Db** resulting in the dihydrogen complexes $(OHCC_2H_4)Co(CO)_3(\eta^2\text{-}H_2)$, **3Ca** and **3Da**, is discussed first. As shown in Figure 12, the incoming H_2 attacks the Co center in side-on orientation (η^2-H_2) and simultaneously breaks the Co···O interaction. In the trigonal bipyramidal transition states **TS(2Cb/3Ca)** and **TS-(2Db/3Da)**, the formylalkyl group stands at the axial site, and the hydrogen ligand occupies the equatorial site. The same conformations have been found in the dihydrogen complexes **3Ca** and **3Da**, in which the H−H bond length is 0.807/0.800 Å, in line with the experimental value (0.82 Å).[48] This activation is mainly caused by the electron donation from the cobalt d orbital to the σ^* (H_2) orbital.[45] In addition, the formation of **3Ca** or **3Da** is predicted to be endergonic by 12.4 or 14.9 kcal/mol, and the former is 3.9 kcal/mol higher in free energy than the latter.

The next step is the formation of the dihydride complexes (**3Cb**/**3Db**) from the oxidative addition. As illustrated in Figure 12, **3Cb** and **3Db** have distorted

(48) Heinekey, D. M.; Oldham, W. J., Jr. *Chem. Rev.* **1993**, *93*, 913.

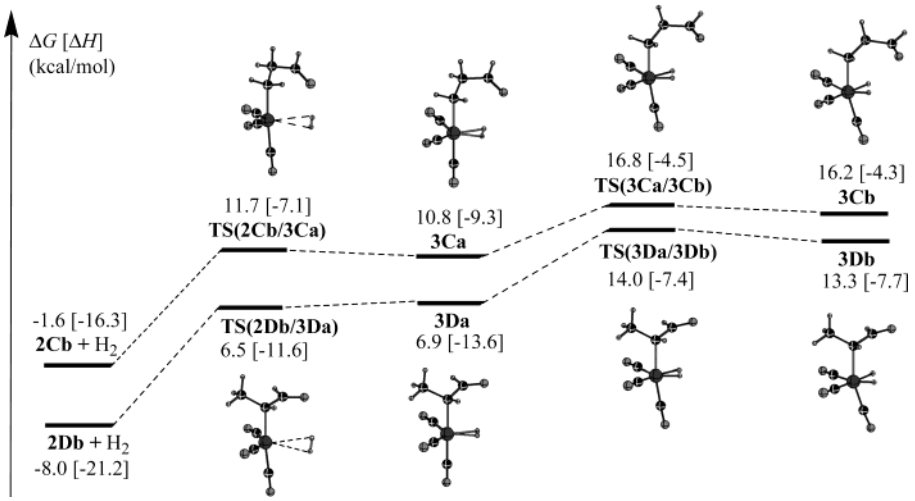

Figure 11. Free energy profiles (kcal/mol, enthalpies in square brackets) for H_2 coordination and oxidative addition of C═C hydrogenation (relative to $HCo(CO)_3$ + acrolein + H_2).

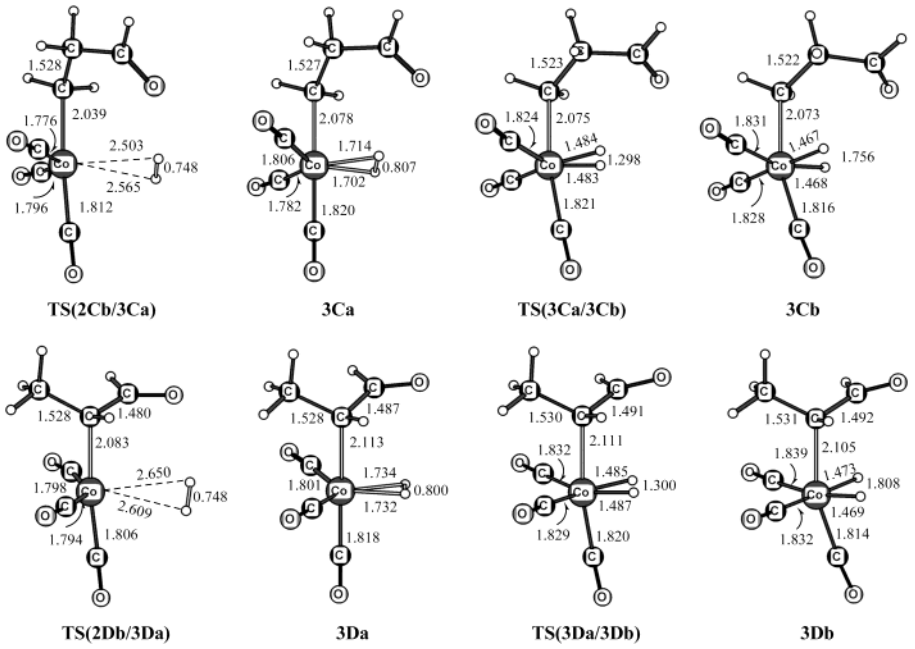

Figure 12. Bond parameters (in Å) of the critical points involved in H_2 coordination and oxidative addition of C═C hydrogenation.

octahedral geometries. Compared with the corresponding η^2-complexes **3Ca** and **3Da**, the main change in **3Cb** and **3Db** is the dissociation of the H−H bond accompanied with the shortening of the Co−H bonds. From the free energy profiles in Figure 11, we can see that the H_2 oxidative addition (**3Ca** → **3Cb** or **3Da** → **3Db**) is endergonic by 5.4 or 6.4 kcal/mol, and **3Db** is more stable than **3Cb** by 2.9 kcal/mol.

(d) Propanal Elimination. The elimination of propanal from **3Cb** or **3Db** proceeds by one of the hydride ligands migrating and attacking the β- or α-carbon atom. The corresponding free energy profiles are reported in Figure 13, while the structures of the critical points are depicted in Figure 14. It is clearly shown that this process proceeds via the three-center transition state **TS(3Cb/4C)** or **TS(3Db/4D)**. In addition, the propanal elimination from the dihydride complex is highly exergonic and occurs easily by overcoming a small free energy barrier (Figure 13).

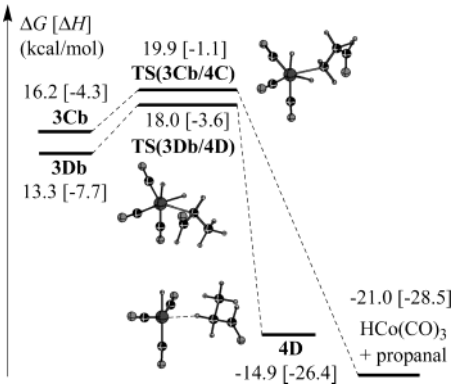

Figure 13. Free energy profiles (kcal/mol, enthalpies in square brackets) for propanal elimination (relative to $HCo(CO)_3$ + acrolein + H_2).

(e) Reaction Pathways for Propanal Formation. On the basis of the results discussed above, both paths

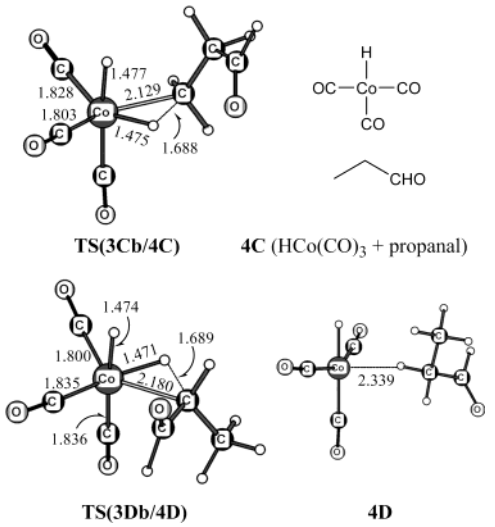

Figure 14. Bond parameters (in Å) of the critical points involved in propanal elimination.

have smooth free energy profiles without thermodynamic traps or insurmountable barriers. The difference in favoring the reaction path is the free energy barrier of the Co−H insertion process. The barrier for path D is 2.4 kcal/mol lower than for path C, and therefore the former is more favored than the latter. In addition, all intermediates along path D are lower in energy than corresponding species along path C. H_2 coordination has the highest barrier of 14.5 kcal/mol and is the rate-determining step.

(3) Chemoselectivity. Two factors can be responsible for the chemoselectivity of acrolein hydrogenation. One is the relative stability of the $HCo(CO)_3$-acrolein complexes, and the other is the overall free energy barrier. Compared with the complex **1a-*end***, the π complex **1c-*syn*** is more stable by 3.5 kcal/mol. Considering a possible equilibrium between **1a-*end*** and **1c-*syn*** on the basis of thermodynamics ($\Delta G = -RT \ln K$), the expected ratio will be 1:99, revealing that acrolein prefers coordination to $HCo(CO)_3$ via the C═C group, leading to its activation. Furthermore, the formation of allyl alcohol by path B (**1a-*end*** → **4B**) has an overall free energy barrier of 36.4 kcal/mol, which is much higher than that of 17.8/17.4 kcal/mol for the formation of propanal along path D (**1c-*syn*/1d-*anti*** → **4D**). As a consequence, the $HCo(CO)_3$-catalyzed hydrogenation of acrolein takes place selectively on the C═C group, and the formation of allyl alcohol is almost suppressed, which is in line with the experimental finding. Therefore, saturated aldehydes are the principal products of the hydrogenation reaction, and the subsequent products are the saturated alcohols.

At this stage, it is also interesting to compare the competing possibility between hydrogenation and hydroformylation of the terminal C═C bond. It is found experimentally[49] that the probability of hydrogenation as a side reaction in hydroformylation depends highly on the structure of the catalysts, the reaction conditions (H_2 and CO partial pressures), and the substituents of alkenes. Our previous study[34] demonstrated that hydroformylation of acetylene is more favored kinetically than hydrogenation. For comparison, the propene hydrogenation was computed. On the basis of their most stable (iso)propyl complexes, we have found that propene hydrogenation has a smaller free energy barrier than acrolein (7.3/9.7 vs 13.3/14.5 kcal/mol), and both reactions are predicted to be endergonic by 8.5/10.5 and 12.4/14.9 kcal/mol, respectively. This indicates the large effect of substituents, and propene can be more easily hydrogenated than acrolein.

In addition to hydrogenation of propene (7.3/9.7 kcal/mol), the competing addition of CO leading to aldehydes was computed to have a similar free energy barrier (7.0/8.9 kcal/mol) and to be highly exergonic (−9.0/−6.3 kcal/mol),[46] while the corresponding H_2 addition is endergonic (8.5/10.5 kcal/mol). This comparison reveals that propene hydroformylation is controlled by thermodynamics, and the hydrogenation process is not competitive. Considering a possible equilibrium between H_2 and CO coordination to the most stable $(C_3H_7)Co(CO)_3$ complex in eq 6, the competitive potential can be obtained from the large endergonic value of 17.5/16.7 kcal/mol, and this indicates that H_2 addition is not competitive thermodynamically.

$$(C_3H_7)Co(CO)_4 + H_2 = (C_3H_7)Co(CO)_3(\eta^2\text{-}H_2) + CO \quad (6)$$

$$\Delta G = 17.5/16.7 \text{ kcal/mol}$$

Conclusion

The complete catalytic cycle of the $HCo(CO)_3$-catalyzed C═O and C═C selective hydrogenation of acrolein has been investigated at the B3LYP/6-311+G(d) density functional level of theory. The acrolein coordination to catalyst $HCo(CO)_3$ can take place via the C═O or C═C group. The coordination of the C═O functional group favors the *end-on* (**1a-*end***) rather than the *side-on* (**1b-*side***) form by 5.9 kcal/mol in free energy. The most stable coordination is the π complex $HCo(CO)_3(\eta^2\text{-}H_2C$═$CHCHO)$ of the C═C bond (**1c-*syn*/1d-*anti***), and this enhanced stability determines the selective hydrogenation of the C═C over the C═O bond. Therefore, propanal is the principal product from C═C hydrogenation, while the production of allyl alcohol is almost suppressed, in line with the experimental finding.

The formation of propanal via the C═C selective hydrogenation of acrolein proceeds along migratory insertion, H_2 coordination, and oxidative addition as well as reductive elimination of propanal. The migratory insertion occurs in two ways, the hydride transfer to C_α or to C_β. In the first case (path C), the hydride transfer to C_α is coupled with the Berry pseudorotation of the skeleton, whereas the hydride transfer to C_β (path D) proceeds by stepping. The whole insertion process (**1d-*anti*** → **2Cb** or **1c-*syn*/1d-*anti*** → **2Db**) is computed to be exergonic by 2.2 or 8.2/8.6 kcal/mol, with the total free energy barriers of 8.7 or 6.3/7.0 kcal/mol, respectively. These results show a preferred C_β attack both kinetically and thermodynamically. In addition, all intermediates along path D are lower in energy than corresponding species along path C. Therefore path D is more favored. The H_2 coordination is computed to be an endergonic process, which determines the rate, and the propanal elimination is a highly exergonic and irreversible process.

(49) Falbe, J. *New Sytheses with Carbon Monoxide*; Springer-Verlag: Berlin, 1980.

For the C═O selective hydrogenation producing allyl alcohol, two possible paths are considered, i.e., reaction through the hydroxyallyl (path A) and allyloxy (path B) intermediates. Prior to the insertion reaction, the complex **1a-*end*** transforms to the π complex **1b-*side***, and the formyl group insertion into the Co−H bond forming the hydroxyallyl complex **2A** or the allyloxy complex **2B** is a slightly endergonic process. Kinetically, the hydride transfer to carbon forming the allyloxy complex **2B** (path B) is more favored than that to oxygen to form the hydroxyallyl complex **2A** (path A), as indicated by the free energy barrier of 8.7 and 24.0 kcal/mol, respectively. Thermodynamically, the overall intermediates of path B are lower in energy than those of path A. Therefore, path A is not competitive to path B, and the formation of allyl alcohol by C═O selective hydrogenation proceeds via the allyloxy intermediate.

Acknowledgment. This work was supported by the Chinese Academy of Sciences (20029908) and the National Natural Science Foundation China.

Supporting Information Available: Total electronic energies and zero-point energies (ZPE) as well as thermal corrections to enthalpies and thermal corrections to Gibbs free energies (403.15 K, 200 atm) for all systems. This material is available free of charge via the Internet at http://pubs.acs.org.

OM034317U